Article

Water-stable Metal-Organic Framework for Hyperpolarized Xenon MRI in Aqueous Solution

ZENG Qingbin[1,2], WANG Zhen[1,2], GUO Qianni[1,2]✉, SONG Wei[1,2], ZHAO Xiuchao[1,2], YANG Yuqi[1,2] and ZHOU Xin[1,2]✉

Received December 9, 2024
Accepted January 22, 2025

Hyperpolarized ^{129}Xe magnetic resonance imaging (MRI) is a powerful tool for detecting respiratory system diseases. However, ^{129}Xe is an inert gas and lacks specific detection capability. Entrapping xenon within molecular cages to enable specific detection is a challenging task, and numerous molecular cages have been developed and evaluated to address this challenge. Herein, we report that the aluminum-based metal-organic framework, CAU-1, can effectively entrap xenon for hyperpolarized ^{129}Xe MRI in aqueous solutions. This platform exhibits high water stability and good dispersibility, and shows excellent xenon entrapment capability, even at a concentration as low as 50 μg/mL. Importantly, it is responsive to pH changes across a range from 6.6 to 5.0, making it promising for monitoring the weakly acidic environment in tumors or metabolic abnormality. Furthermore, the scalable and cost-effective production of this molecular cage will facilitate future advancements in molecular imaging and chemical sensing applications.

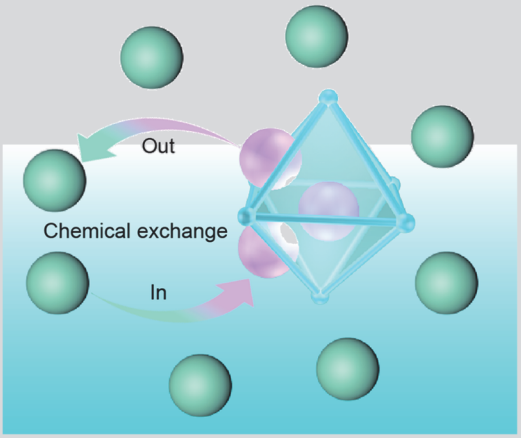

Keywords Metal-organic framework (MOF); Hyperpolarization; Magnetic resonance imaging (MRI)

1 Introduction

Xenon is a non-toxic gas that is soluble in biological fluids and has been widely used as a probe to investigate protein surfaces and the structure of porous materials.[1−6] The nuclear spin of ^{129}Xe can be hyperpolarized through spin-exchange optical pumping (SEOP), resulting in 4—5 orders of magnitude enhancement in nuclear magnetic resonance (NMR) signals, which allows for imaging of lung and brain diseases.[7−14] However, ^{129}Xe is an inert gas and does not inherently enable specific detection or molecular-level imaging. When trapped within molecular cages, xenon atoms exhibit a characteristic peak distinct from dissolved xenon or xenon gas. This provides a promising avenue for hyperpolarized ^{129}Xe magnetic resonance imaging (MRI) as a potential molecular imaging modality.[15] Several molecular cages, including cryptophane-A (CryA),[16] cucurbit[6]uril (CB[6]),[17] nanoemulsion,[18] gas vesicles,[19] proteins,[20] metal-organic capsules,[21] metal-organic layers,[22] pillar[5]arenes,[23] and Noria derivative,[24] have been developed for trapping xenon atoms in hyperpolarized ^{129}Xe NMR. CryA is one of the most widely used molecular cages for xenon entrapment. However, its complex synthesis and low water solubility are significant limitations. Similarly, CB[6], another well-known xenon host molecular cage, suffers from poor water solubility and difficulties in functionalization, which limits its application in biosensing. Consequently, developing novel molecular cages for xenon entrapment has attracted significant attention.

Microporous materials, such as metal-organic frameworks (MOFs), with high internal surface areas and pore volumes can concentrate gas molecules through adsorption. These materials possess rich and ordered porosity, and have been developed for gas storage and separation.[25−30] Nearly all MOFs exhibit affinity for gas molecules, and many have been used for xenon gas adsorption and separation in the solid state.[31−35] In the previous study, we demonstrated that the ZIF-8, IRMOF-1, IRMOF-8, and IRMOF-10 can entrap xenon atoms in

✉ GUO Qianni
qian-niguo@wipm.ac.cn
✉ ZHOU Xin
xinzhou@wipm.ac.cn
1. State Key Laboratory of Magnetic Resonance Spectroscopy and Imaging, National Center for Magnetic Resonance in Wuhan, Wuhan Institute of Physics and Mathematics, Innovation Academy for Precision Measurement Science and Technology, Chinese Academy of Sciences, Wuhan 430071, P. R. China;
2. University of Chinese Academy of Sciences, Beijing 100049, P. R. China

https://doi.org/10.1007/s40242-025-4234-6

solutions.[36,37] However, the xenon entrapment capability of these MOFs was significantly reduced when dispersed in aqueous solution due to factors, such as dispersity, water stability, and other related issues. To the best of our knowledge, only ZIF-8 has exhibited a strong affinity for xenon atoms in aqueous solution to date.[36]

A well-known aluminum-based metal-organic framework (MOF), CAU-1, shows good thermal stability and water stability.[38] Moreover, aluminum, as a metal source for MOF construction, is cost-effective and safe due to its abundance and low toxicity. This MOF consists of AlO_6 octahedra that connect to eight rings, alternately sharing corners and edges. These inorganic building units are linked by twelve 2-aminoterephthalate ions, forming a tetragonal structure with two types of cages: distorted octahedral and distorted tetrahedral, which have effectively accessible diameters of approximately 10 and 4.5 Å (1 Å=0.1 nm), respectively (Fig. 1B). Each cage features small triangular windows with a free aperture of 3—4 Å (Fig. 1B), which provides the only possible access to the cages (Fig. 1). Previous studies have demonstrated that CAU-1 can adsorb xenon atoms in the solid state, with the adsorbed ^{129}Xe exhibiting a characteristic peak at a chemical shift of approximately 75 ppm.[39] This unambiguously confirms that xenon atoms can access the cages through the triangular windows of CAU-1. However, whether the CAU-1 can trap xenon atoms in aqueous solution remains unexplored.

Herein, we demonstrate for the first time that CAU-1 could trap xenon atoms in aqueous solution and generate a strong hyperpolarized ^{129}Xe signal for MRI at low concentrations. More importantly, the NMR signal of ^{129}Xe entrapped in CAU-1 exhibits a robust pH response over a wide range. Aluminum ions and amino groups on the surface of CAU-1 facilitate excellent dispersion of these MOF nanoparticles in water, with the amino groups providing pH-responsive functionality. These characteristics make CAU-1 an excellent molecular cage for trapping xenon atoms for hyperpolarized ^{129}Xe MRI. Overall, we present a new platform for encapsulating xenon atoms for MRI, expanding the toolbox of ^{129}Xe molecular cages.

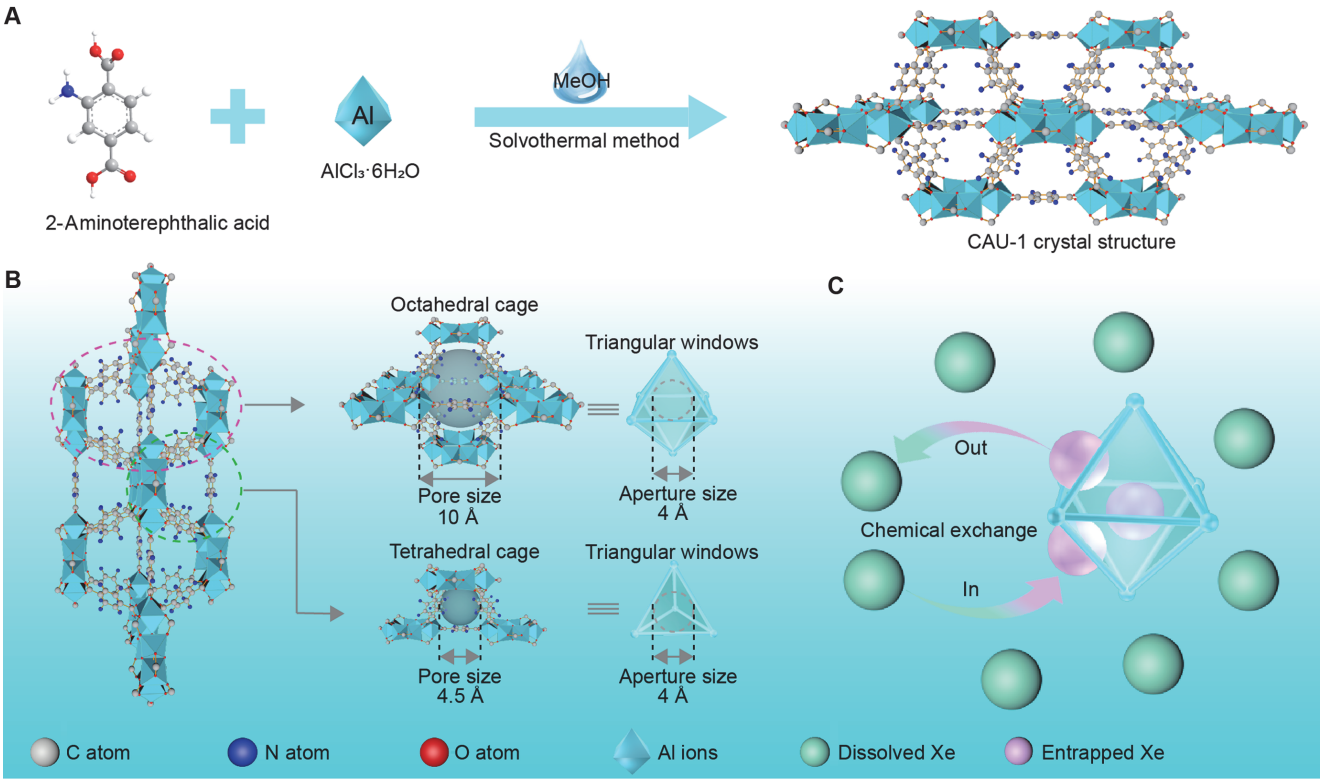

Fig. 1 Illustrations for the CAU-1 utilized to trap xenon atoms in aqueous solutions

(A) CAU-1 was synthesized using a solvothermal method in methanol; (B) CAU-1 contains two distinct cages, a distorted octahedral cage with a 10 Å (1 Å=0.1 nm) pore and a tetrahedral cage with a 4.5 Å pore; (C) xenon atoms enter the cages through the triangular windows of CAU-1, and the dissolved Xe will exchange with the entrapped Xe in CAU-1.

2 Experimental

2.1 Materials and Measurements

Aluminum chloride hexahydrate ($AlCl_3·6H_2O$), anhydrous methanol, anhydrous ethanol, *N*,*N*-dimethylformamide (DMF) were purchased from Sinopharm Chemical Reagent Co., Ltd. (Shanghai). 2-Amino-terephthalic acid was purchased from Aladdin (Shanghai, China). All chemicals were commercially obtained and used without further purification. Transmission electron microscope (TEM, JEM-2100 JOEL Company, Janpan), scanning electron microscope

https://doi.org/10.1007/s40242-025-4234-6

(SEM, Gemini SEM 500, ZEISS Company, Germany), powder X-ray diffraction instrument (PXRD, Bruker D8, Bruker Company, Germany), N_2 adsorption analysis instrument (BELSORP-max), Fourier transform infrared spectroscope (FTIR, Thermo Scientific Nicolet iS10, Thermo Company, USA), thermal gravimetric analysis instrument (TGA, TGA Q500, TA Company, USA), dynamic light scattering detector (DLS, Zetasizer Nano ZS90, Malvern Company, UK). ^{129}Xe NMR and ^{129}Xe MRI experiments were carried out using a 400 MHz Bruker AV400 wide-bore spectrometer (Bruker Biospin, Ettlingen, Germany).

2.2 Preparation of CAU-1

Aluminum chloride hexahydrate and 2-aminoterephthalic acid were dissolved in methanol using ultrasound, then transferred to a Teflon-lined stainless-steel autoclave (15 mL) and heated at 125 °C for 5.5 h. After gently cooling to room temperature, the solution was centrifuged at 10000 rpm for 5 min, and the solid collected at the bottom was further washed twice with DMF and methanol, respectively. Finally, it was heated in a vacuum-drying oven at 50 °C for 24 h. The particle sizes were controlled by altering the concentration of organic ligands and metal salts. The quantities of the initial materials are shown in the Electronic Supplementary Information (ESI).

2.3 Hyperpolarized Chemical Exchange Saturation Transfer (Hyper-CEST) Spectra

The hyperpolarized gas mixture was introduced into a 10 mm NMR tube for 20 s, followed by a 3 s delay to allow the bubbles to collapse. The ^{129}Xe NMR spectra were acquired after the ^{129}Xe within the CAU-1 was saturated by a continuous-wave pulse (6.5 μT, 10 s). All ^{129}Xe NMR spectra were acquired in a single scan and processed using Lorentzian broadening (LB=5 Hz).

2.4 Hyper-CEST MRI

Images were obtained using a RARE sequence (slice thickness=30 mm, field of view=30 mm×30 mm, matrix size=32×32, in-plane resolution=0.9375 mm×0.9375 mm, bandwidth=5400 Hz, echo time=4.97 ms, repetition time=28080 ms, centric *k*-space encoding, no partial Fourier transform acceleration, RARE factor=8). Sixteen on-resonant and sixteen off-resonant scans were acquired and averaged. For each excitation, after the hyperpolarized ^{129}Xe was bubbled into the solution for 20 s, a 3 s delay was included to allow the bubbles to collapse. Before imaging, a saturation pulse (13 μT, 5 s) was applied to saturating the on-resonant (δ −41 relative to dissolved ^{129}Xe in solution at δ 0) or off-resonant (δ 41 relative to dissolved ^{129}Xe in solution at δ 0). The images were processed using MATLAB (R2014a; MathWorks), with the 32×32 image matrix interpolated into a 64×64 matrix. The Hyper-CEST effect for on-resonant saturation was analyzed in comparison to off-resonant saturation for each pixel using the formula [CEST effect=($Intensity_{off}$-$Intensity_{on}$)/$Intensity_{off}$] on a point-by-point basis.

3 Results and Discussion

3.1 Synthesis and Characterization of CAU-1

A series of CAU-1 was synthesized *via* the solvothermal method in methanol, with particle sizes precisely tuned by altering the concentration of organic ligands. The morphology and particle size of these CAU-1 were characterized using the scanning electron microscope (SEM) and the transmission electron microscope (TEM). SEM analysis shows that different experiment conditions lead to MOFs with gradually increased particle sizes, 60, 120, 250, 320, and 510 nm, respectively (Fig. 2A, and Figs. S1—S5 in the ESI). Additionally, SEM and TEM images reveal that these particles exhibit a rice kernel shape with smooth surfaces (Fig. 2, A and B). Elemental mapping confirmed the homogeneous distribution of Al within the framework (Fig. 2C). Powder X-ray diffraction (PXRD) patterns indicate that the diffraction peaks of these MOFs matched well with the simulated pattern based on the single-crystal structure of CAU-1, without any extra diffraction peaks, confirming the phase purity and high crystallinity of these MOFs (Fig. S6 in the ESI). Fourier-transform infrared (FTIR) spectroscopy revealed that the stretching vibration absorption peak around 3000 cm^{-1} (hydroxyl vibration in —COOH) disappeared, and the redshift of the peak at 1675 cm^{-1} (C═O stretching vibration), suggests that Al^{3+} coordinates with the —COOH groups in the organic ligands (Fig. S7 in the ESI). Nitrogen adsorption isotherms at 77 K were performed to determine the permanent porosity of these MOFs. Desolvated MOFs display a Brunauer-Emmett-Teller surface area of 1231—1498 m^2/g (Figs. S8—S22 and Table S1 in the ESI). Nonlocal density functional theory calculations of the pore size distribution showed peaks around 0.6 and 0.8 nm (Table S1), consistent with previous reports.[40] Thermo gravimetric analysis curves showed no significant mass loss before 300 °C (Fig. S23 in the ESI), indicating the high thermal stability of these MOFs and confirming the complete removal of solvent.

3.2 Nanoparticle Size-dependent Hyper-CEST

Solvent-free CAU-1 was used to obtain hyperpolarized ^{129}Xe

https://doi.org/10.1007/s40242-025-4234-6

NMR in the solid state. A strong ^{129}Xe NMR signal appeared at approximately δ 88, attributed to the xenon atoms entrapped within the CAU-1 pores (Fig. 2D). This finding is consistent with the previous study.[38] Subsequently, CAU-1 was dispersed in aqueous solution at a high concentration (5 mg/mL), and the hyperpolarized ^{129}Xe NMR experiment was performed. A ^{129}Xe NMR signal appeared at δ 193, attributed to the dissolved ^{129}Xe. However, no additional signals were observed in the ^{129}Xe NMR spectrum (Fig. 2D). This result suggests that the xenon atoms entrapped within CAU-1 are not readily detectable by NMR under the experimental conditions.

To overcome this limitation, an indirect detection method, hyperpolarized xenon chemical exchange saturation transfer (Hyper-CEST),[41] was employed to investigate CAU-1 at low concentrations. The Hyper-CEST method exploits the exchange of ^{129}Xe populations between the bulk aqueous solution and the molecular cages. This is achieved by selectively saturating the bound signal. When a saturation pulse is applied at the resonance frequency of entrapped ^{129}Xe, the ^{129}Xe nuclei become depolarized, resulting in a corresponding depletion of the signal from dissolved ^{129}Xe, which can be easily monitored. This signal was compared to a reference measurement that utilized an "off-resonance" saturation to account for the natural self-relaxation of dissolved hyperpolarized ^{129}Xe over time. Interestingly, the Hyper-CEST spectrum revealed two distinct saturation responses (Fig. 2E). The first response

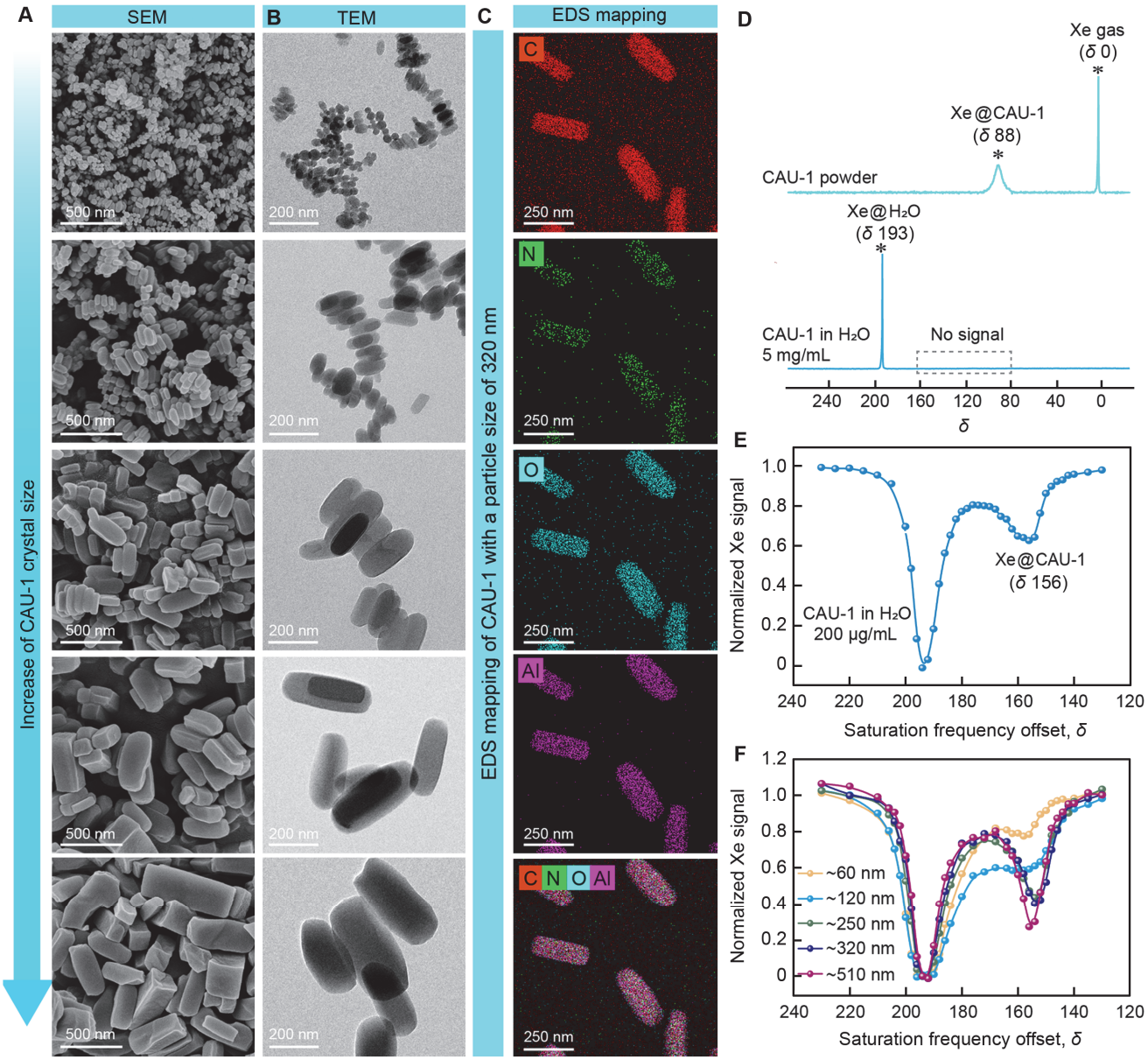

Fig. 2 Morphology Images and hyperpolarized ^{129}Xe NMR spectra of CAU-1

(A) SEM images of a series of CAU-1; (B) TEM images of a series of CAU-1; (C) elemental mapping of CAU-1 with a particle size of 320 nm; (D) hyperpolarized ^{129}Xe NMR spectra of CAU-1 nanoparticles in aqueous solution and solid state; (E) hyperpolarized ^{129}Xe NMR spectra obtained by the Hyper-CEST method for CAU-1 (200 μg/mL) with a particle size of 120 nm in aqueous solution; (F) Hyper-CEST spectra of a series of CAU-1 (200 μg/mL) with different nanoparticle sizes in aqueous solution.

https://doi.org/10.1007/s40242-025-4234-6

was attributed to the direct saturation of free dissolved ^{129}Xe, centered at δ 193, while the second response, located at δ 154, resulted from the ^{129}Xe trapped within CAU-1. The chemical shift of the entrapped ^{129}Xe in CAU-1 showed a significant difference between its behavior in the aqueous solution and the solid state. This variation may arise from water molecules that have entered the pores of CAU-1 or those involved in hydrogen bonding with the framework. Despite the low concentration of CAU-1 (200 μg/mL), the observed Hyper-CEST effect was approximately 40%. This finding unambiguously demonstrated that CAU-1 can be used as an effective molecular cage for the entrapment of xenon atoms in hyperpolarized ^{129}Xe NMR.

The particle size plays a crucial role in determining the properties of nanoparticles, as nanoparticles of different sizes exhibit distinct characteristics. To investigate the influence of MOF size on xenon entrapment capability, a series of MOFs with varying sizes was synthesized by adjusting the reactant concentrations and reaction time. The solvent-free MOFs were then used to perform Hyper-CEST experiments in aqueous solution. The results demonstrated that the Hyper-CEST effect varied with particle size, increasing within an optimal size range (Fig. 2F). We hypothesized that if the MOF sizes are too small, there may be insufficient pores to effectively capture xenon atoms, combined with the rapid exchange between entrapped and dissolved xenon and a short relaxation time, leading to a weak Hyper-CEST effect. On the other hand, MOFs within a suitable size range are likely to have enough pores to capture xenon atoms, along with a longer relaxation time, which together result in a strong Hyper-CEST effect. It is also known that particle size influences nanoparticle dispersity and biocompatibility. Larger particles tend to exhibit lower dispersity and biocompatibility, which could limit their applicability in biological systems. Considering these factors, Hyper-CEST effect, dispersity, and biocompatibility, we determined that the optimal particle size for CAU-1 is around 320 nm. Subsequent experiments were conducted using CAU-1 of this size.

3.3 Evaluation of Hyper-CEST Performance

To further investigate the Hyper-CEST performance of the MOFs, various concentrations of CAU-1 were dispersed in aqueous solution, and Hyper-CEST experiments were performed (Fig. 3). The results showed that as the concentration of CAU-1 particles increased, the Hyper-CEST effect exhibited a linear relationship within the concentration range from 50 μg/mL to 250 μg/mL (Fig. 3, A and B). Remarkably, even at a low concentration of 50 μg/mL, the Hyper-CEST effect remains substantial, reaching approximately 20%. To achieve the 20% Hyper-CEST effect, the concentration of CAU-1 is four times lower than that of IRMOF-1.[36] This highlights the excellent Hyper-CEST performance of CAU-1 nanoparticles at ultralow concentrations. Furthermore, the corresponding Hyper-CEST MRI also demonstrated a good linear correlation between MRI signal intensity and CAU-1 nanoparticle concentration (Fig. 3C, Fig. S24 and Fig. S25 in the ESI). These results emphasize the remarkable potential and high sensitivity of CAU-1 nanoparticles, even at ultralow concentrations. This suggests promising applications for

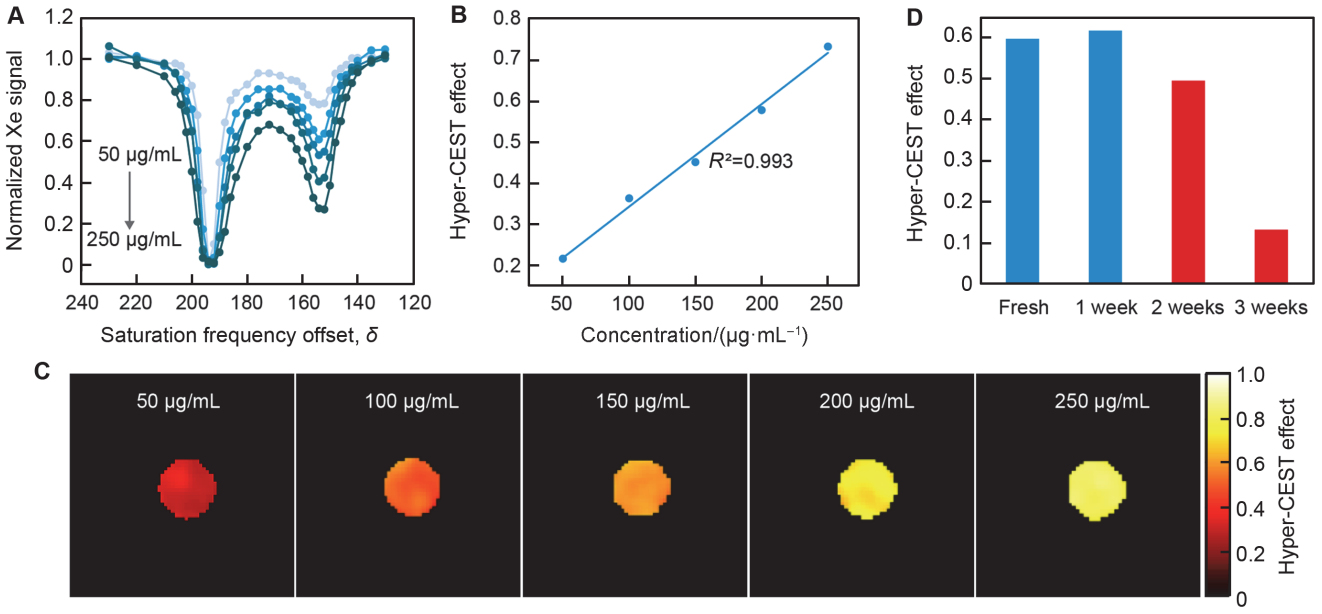

Fig. 3 Hyperpolarized ^{129}Xe NMR and MRI of CAU-1

(A) Hyper-CEST spectra for different concentrations of CAU-1 nanoparticles (50, 100, 150, 200, and 250 μg/mL); (B) concentration-dependent Hyper-CEST effect at δ 152 for CAU-1; (C) Hyper-CEST MRI of CAU-1 nanoparticles at different concentrations; (D) Hyper-CEST effect at δ 152 for CAU-1 after immersion in water for various time.

https://doi.org/10.1007/s40242-025-4234-6

these nanoparticles in Hyper-CEST MRI, where their exceptional performance could open new avenues for highly sensitive low-concentration molecular imaging.

3.4 Evaluation of Water Stability

Furthermore, after immersing CAU-1 in water for one week, its morphology (Fig. S26 in the ESI) and Hyper-CEST effect (Fig. 3D, Fig. S27 in the ESI) showed no significant changes compared to the freshly prepared sample. However, after more than two weeks of immersion, the Hyper-CEST effect significantly decreased, while the morphology and crystal structure remained unchanged even after four weeks (Figs. S26 and S28). This decrease in the Hyper-CEST effect may be due to more water molecules and CO_2 entering the pores of CAU-1.[42] Nevertheless, the water stability of CAU-1 after one week holds great promise for its use in biomedical applications.

3.5 Quantitative of Exchange Rate

Additionally, Hyper-CEST spectra were measured for CAU-1 at the same concentrations using varying saturation pulses (B_1 field of 8.0, 6.5, 4.0 μT). A full series of Hyper-CEST spectra were obtained by saturating the entrapped ^{129}Xe within CAU-1. After fitting the data to McConnell–Bloch equations, the exchange rate of ^{129}Xe from CAU-1 pores to the aqueous solution was determined to be (6155±847) Hz (Fig. S29 in the ESI).

3.6 pH-Response in Aqueous Solution

Finally, given that CAU-1 contains large numbers of amino groups, the zeta potential, nanoparticle sizes, and Hyper-CEST spectra were measured in aqueous solutions with varying pH. As the pH decreased from 6.6 to 3.0, the zeta potential increased dramatically from 23 mV to 47 mV (Figs. S30—S35). This suggests that CAU-1 undergoes protonation at pH values below 6.6. It is worth noting that, as the pH decreased from 5.0 to 4.0, the zeta potential remained unchanged, suggesting that CAU-1 may not undergo further protonation in this range. Below pH 4.0, the zeta potential increases significantly again as the pH decreases. Dynamic light scattering (DLS) measurements showed that the particle sizes of CAU-1 in aqueous solution decreased slightly as the pH decreased from 6.6 to 5.0. However, when the pH is below 5.0, the particle sizes remain unchanged, suggesting that the CAU-1 is stable in an acidic solution (Figs. S36—S40).

For the Hyper-CEST, both the chemical shift of the saturation peak and the Hyper-CEST effect demonstrated a clear response to changes in pH (Fig. 4). At pH 6.6, the saturation peak is centered at δ 156, and the Hyper-CEST effect is 0.43 (Fig. 4A). As the pH of the solution decreased from neutral to acidic, the saturation peak shifted upfield, and the Hyper-CEST effect increased significantly. When the pH is reduced from 6.6 to 3.0, the saturation peak moves from δ 156 to δ 152, while the Hyper-CEST effect rises to 0.73 (Fig. 4A). Both the chemical shift of the saturation peak and the Hyper-CEST effect show nonlinear behavior as a function of pH (Fig. 4, B and C). The pH dependence of Hyper-CEST is similar to that of the zeta potential (Fig. 4B and Fig. S35). These results suggest that protonation of CAU-1 may affect the interaction between xenon atoms and the framework. We hypothesize that protonation of the amino groups in the framework could disrupt the hydrogen bonds between water molecules and the framework, which could influence the chemical exchange between the entrapped xenon and dissolved xenon, thereby enhancing the Hyper-CEST effect. Additionally, protonation of the amino groups may alter the interaction between xenon atoms and the framework, resulting in an upfield shift of the saturation peak. Notably, within the pH range of 6.6 to 5.0, both the Hyper-CEST and chemical shift exhibit a sensitive, linear response to pH changes (Fig. 4, B and C). Specifically,

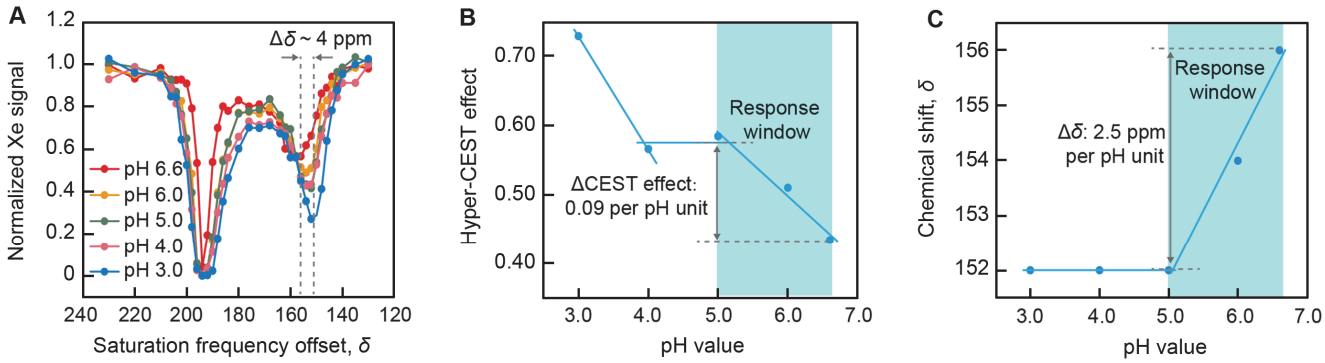

Fig. 4 Hyper-CEST spectrum of CAU-1 (200 μg/mL) at different pH values in aqueous solution
(A) pH-dependent Hyper-CEST spectra of CAU-1; (B) plot of the Hyper-CEST effect at saturation peak versus pH; (C) chemical shift of the saturation peak *versus* pH.

https://doi.org/10.1007/s40242-025-4234-6

the Hyper-CEST effect changes by 0.09 per unit pH change, while the chemical shift of the saturation peak varies by δ 2.5 per pH unit. The observed chemical shift difference is larger than state-of-the-art CryA modified with pH-sensitive moiety.[43] The wide range and substantial chemical shift difference suggest great potential for using this system in pH detection in biological systems in the future.

4 Conclusions

In summary, we report that CAU-1, a new type of MOF, can serve as an effective molecular cage for entrapping xenon atoms in aqueous solutions. This system, which demonstrates high water stability and dispersibility, shows excellent xenon entrapment capability even at low concentrations. Specifically, at ultralow concentrations (50 μg/mL), the Hyper-CEST effect is approximately 20%. Importantly, CAU-1 exhibits a strong and broad pH response, making it a promising candidate for pH detection in biological systems. Thus, we have expanded the molecular cages toolbox and provided an additional option for hyperpolarized ^{129}Xe MRI applications. Further studies on CAU-1 are expected to focus on several areas, including but not limited to the following. First, functionalizing CAU-1 with other moieties to fine-tune its pH response range makes it more suitable for pH detection in biological systems. Second, incorporating targeting groups into CAU-1 enables the detection of biomolecules *via* hyperpolarized ^{129}Xe NMR. Third, introducing multivariate building units into the CAU-1 structure modulates the interaction of xenon atoms with the framework, thereby enhancing the NMR signal intensity of entrapped ^{129}Xe.

Electronic Supplementary Information

Supplementary material is available in the online version of this article at http://dx.doi.org/10.1007/s40242-025-4234-6.

Acknowledgements

This work was supported by the National Natural Science Foundation of China (Nos. 82127802, 21921004), the Strategic Priority Research Program of CAS (No. XDB0540000), the Key Research Program of Frontier Sciences of CAS (No. ZDBS-LY-JSC004), the Key Technology Foundation of Hubei Province, China (No. 2021ACA013), the Major Program (JD) of Hubei Province, China (No. 2023BAA021), the CAS Fund for the Youth Interdisciplinary Team, China (No. JCTD-2022-13), the Youth Innovation Promotion Association of CAS (No. 2023347), Wuhan Talent Project, China and the Natural Science Foundation of Hubei Province, China (No. 2023AFB790).

Conflicts of Interest

The authors declare no conflicts of interest.

References

[1] Wiebelhaus N., Singh N., Zhang P., Craig S. L., Beratan D. N., Fitzgerald M. C., *J. Am. Chem. Soc.,* **2022**, *144*, 3925.
[2] Blobel J., Schmidl S., Vidal D., Nisius L., Bernadó P., Millet O., Brunner E., Pons M., *J. Am. Chem. Soc.,* **2007**, *129*, 5946.
[3] Dubois L., Silva P. D., Landon C., Huber J. G., Ponchet M., Vovelle F., Berthault P., Desvaux H., *J. Am. Chem. Soc.,* **2004**, *126*, 15738.
[4] Li J., Léonce E., Coutellier C., Boutin C., Chighine K., Rivron C., Davidson A., Berthault P., *Anal. Chem.,* **2024**, *96*, 9430.
[5] Mailhiot S. E., Peuravaara P., Egleston B. D., Kearsey R. J., Mareš J., Komulainen S., Selent A., Kantola A. M., Cooper A. I., Vaara J., Greenaway R. L., Lantto P., Telkki V.-V., *J. Phys. Chem. Lett.,* **2024**, *15*, 5323.
[6] Zhou B., Komulainen S., Vaara J., Telkki V.-V., *Micropor. Mesopor. Mater.*, **2017**, *253*, 49.
[7] Mugler J. P., Altes T. A., *J. Magn. Reson. Imaging*, **2013**, *37*, 313.
[8] Li H., Zhao X., Wang Y., Lou X., Chen S., Deng H., Shi L., Xie J., Tang D., Zhao J., Bouchard L.-S., Xia L., Zhou X., *Sci. Adv.*, **2021**, *7*, eabc8180.
[9] Fang Y., Li H., Shen L., Zhang M., Luo M., Li H., Rao Q., Chen Q., Li Y., Li Z., Zhao X., Shi L., Zhou Q., Han Y., Guo F., Zhou X., *Magn. Reson. Med.*, **2024**, *92*, 956.
[10] Rao Q., Li H., Zhou Q., Zhang M., Zhao X., Shi L., Xie J., Fan L., Han Y., Guo F., Liu S., Zhou X., *Eur. Radiol.*, **2024**, *34*, 7450.
[11] Zhou Q., Rao Q., Li H., Zhang M., Zhao X., Shi L., Ye C., Zhou X., *Magn. Reson. Lett.*, **2021**, *1*, 2.
[12] Shepelytskyi Y., Grynko V., Li T., Hassan A., Granberg K., Albert M. S., *Magn. Reson. Med.*, **2021**, *86*, 3147.
[13] Friedlander Y., Zanette B., Lindenmaier A., Li D., Kadlecek S., Santyr G., Kassner A., *Magn. Reson. Med.*, **2022**, *87*, 1971.
[14] Collier G. J., Schulte R. F., Rao M., Norquay G., Ball J., Wild J. M., *Magn. Reson. Med.*, **2023**, *89*, 2217.
[15] Yang Y., Yue S., Shen L., Dong H., Li H., Zhao X., Guo Q., Zhou X., *Adv. Sci.*, **2025**, doi.org/10.1002/advs.202413426.
[16] Spence M. M., Rubin S. M., Dimitrov I. E., Ruiz E. J., Wemmer D. E., Pines A., Yao S., Tian F., Schultz P. G., *Proc. Natl. Acad. Sci. USA*, **2001**, *98*, 10654.
[17] Kunth M., Witte C., Hennig A., Schröder L., *Chem. Sci.*, **2015**, *6*, 6069.
[18] Stevens T. K., Ramirez R. M., Pines A., *J. Am. Chem. Soc.,* **2013**, *135*, 9576.
[19] Shapiro M. G., Ramirez R. M., Sperling L. J., Sun G., Sun J., Pines A., Schaffer D. V., Bajaj V. S., *Nat. Chem.,* **2014**, *6*, 630.
[20] Wang Y., Roose B. W., Palovcak E. J., Carnevale V., Dmochowski I. J., *Angew. Chem. Int. Ed.,* **2016**, *55*, 8984.
[21] Roukala J., Zhu J., Giri C., Rissanen K., Lantto P., Telkki V.-V., *J. Am. Chem. Soc.,* **2015**, *137*, 2464.
[22] Zhang X., Yang Y., Yuan Y., Yue S., Zhao X., Yue Q., Zeng Q., Guo Q., Zhou X., *Anal. Chem.,* **2024,** *96*, 10152.
[23] Schnurr M., Joseph R., Naugolny-Keisar A., Kaizerman-Kane D., Bogdanoff N., Schuenke P., Cohen Y., Schröder L., *ChemPhysChem,* **2019**, *20*, 246.
[24] Shepelytskyi Y., Grynko V., Batarchuk V., Hasselbrink C. L., Kovacs A. H., Ruset I. C., Rodriguez K., Taradeh N. A., Talwar T., DeBoef B., Albert M. S., *ACS Sensors,* **2023**, *8*, 4707.
[25] Kim D. W., Jung M., Shin D. Y., Kim N., Park J., Lee J.-H., Oh H., Hong C. S., *Chem. Engineer. J.*, **2024**, *489*, 151500.
[26] Yu B., Tao Y., Yao X., Jin Y., Liu S., Xu T., Wang H., Wu H., Zhou W., Zhou X., Ding X., Wang X., Xiao X., Zhang Y., Jiang J., *J. Am. Chem. Soc.*, **2024**, *146*, 28932.
[27] Zhang Y., Han Y., Luan B., Wang L., Yang W., Jiang Y., Ben T., He Y., Chen B., *J. Am. Chem. Soc.*, **2024**, *146*, 17220.
[28] Chen Z., Mian M. R., Lee S.-J., Chen H., Zhang X., Kirlikovali K. O., Shulda S., Melix P., Rosen A. S., Parilla P. A., Gennett T., Snurr R. Q., Islamoglu T., Yildirim T., Farha O. K., *J. Am. Chem. Soc.*, **2021**, *143*, 18838.
[29] Jones N. B., Gibbons B., Morris A. J., Morris J. R., Troya D., *ACS Appl. Mater. Inter.,* **2022**, *14*, 8322.
[30] Erdosy D. P., Wenny M. B., Cho J., DelRe C., Walter M. V.,

Jiménez-Ángeles F., Qiao B., Sanchez R., Peng Y., Polizzotti B. D., Cruz M. O., Mason J. A., *Nature*, **2022**, *608*, 712.

[31] Pei J., Gu X., Liang C., Chen B., Li B., Qian G., *J. Am. Chem. Soc.,* **2022**, *144*, 3200.

[32] Li L., Guo L., Zhang Z., Yang Q., Yang Y., Bao Z., Ren Q., Li J., *J. Am. Chem. Soc.,* **2019,** *141*, 9358.

[33] Gong W., Xie Y., Pham T. D., Shetty S., Son F. A., Idrees K. B., Chen Z., Xie H., Liu Y., Snurr R. Q., Chen B., Alameddine B., Cui Y., Farha O. K., *J. Am. Chem. Soc.,* **2022**, *144*, 3737.

[34] Banerjee D., Simon C. M., Plonka A. M., Motkuri R. K., Liu J., Chen X., Smit B., Parise J. B., Haranczyk M., Thallapally P. K., *Nat. Commun.,* **2016**, *7*, 11831.

[35] Bunzen H., Kolbe F., Kalytta-Mewes A., Sastre G., Brunner E., Volkmer D., *J. Am. Chem. Soc.,* **2018,** *140*, 10191.

[36] Zeng Q., Bie B., Guo Q., Yuan Y., Han Q., Han X., Chen M., Zhang X., Yang Y., Liu M., Liu P., Deng H., Zhou X., *Proc. Natl. Acad. Sci. USA*, **2020**, *117*, 17558.

[37] Yang Y., Zhang Y., Wang B., Guo Q., Yuan Y., Jiang W., Shi L., Yang M., Chen S., Lou X., Zhou X., *Chem. Sci.*, **2021**, *12*, 4300.

[38] Ahnfeldt T., Guillou N., Gunzelmann D., Margiolaki I., Loiseau T., Férey G., Senker J., Stock N., *Angew. Chem. Int. Ed.*, **2009**, *48*, 5163.

[39] Kemnitzer T. W., Tschense C. B. L., Wittmann T., Rössler E. A., Senker J., *Langmuir,* **2018,** *34*, 12538.

[40] Zhang J., Li P., Zhang X., Ma X., Wang B., *ACS Appl. Mater. Inter.,* **2020,** *12*, 46057.

[41] Schröder L., Lowery T. J., Hilty C., Wemmer D. E., Pines A., *Science,* **2006***, 314*, 446.

[42] Yin H., Wang J., Xie Z., Yang J., Bai J., Lu J., Zhang Y., Yin D., Lin J. Y., *Chem. Commun*., **2014**, *50*, 3699.

[43] Riggle B. A., Wang Y., Dmochowski I. J., *J. Am. Chem. Soc.,* **2015,** *137*, 5542.

https://doi.org/10.1007/s40242-025-4234-6